Atmos. Chem. Phys. Discuss., 13, 8939–8984, 2013
www.atmos-chem-phys-discuss.net/13/8939/2013/
doi:10.5194/acpd-13-8939-2013


Atmospheric Chemistry and Physics Discussions



# Effects of relative humidity on aerosol light scattering: results from different European sites

**P. Zieger, R. Fierz-Schmidhauser, E. Weingartner, and U. Baltensperger**

Paul Scherrer Institute, Laboratory of Atmospheric Chemistry, 5232 Villigen, Switzerland

Received: 17 March 2013 – Accepted: 25 March 2013 – Published: 4 April 2013

Correspondence to: P. Zieger (paul.zieger@alumni.ethz.ch)

Published by Copernicus Publications on behalf of the European Geosciences Union.







## Abstract

The effect of aerosol water uptake on the aerosol particle light scattering coefficient ($\sigma_{sp}$) is described in this study by comparing measurements from five European sites: the Jungfraujoch, located in the Swiss Alps at 3580 m a.s.l., Ny-Ålesund, located on Spitsbergen in the Arctic, Mace Head, a coastal site in Ireland, Cabauw, a rural site in the Netherlands and Melpitz, a regional background site in Eastern Germany. These sites were selected according to the aerosol type usually encountered at that location. The scattering enhancement factor $f(\mathrm{RH},\lambda)$ is the key parameter to describe the effect of water uptake on the particle light scattering. It is defined as the $\sigma_{sp}(\mathrm{RH})$ at a certain relative humidity (RH) and wavelength $\lambda$ divided by its dry value. $f(\mathrm{RH})$ largely varied at the five sites starting from very low values of $f(\mathrm{RH}=85\,\%,\lambda=550\,\mathrm{nm})$ around 1.28 for mineral dust to 3.41 for Arctic aerosol. Hysteresis behavior was observed at all sites except at the Jungfraujoch due to the absence of sea salt. Closure studies and Mie simulations showed that both size and chemical composition determine the magnitude of $f(\mathrm{RH})$. Both parameters are also needed to successfully predict $f(\mathrm{RH})$. Finally, the measurement results were compared to the widely used aerosol model OPAC (Hess et al., 1998). Significant discrepancies were seen especially at intermediate RH ranges, which were mainly attributed to inappropriate implemented hygroscopic growth within OPAC. Replacement of the hygroscopic growth with recent literature values showed a clear improvement of the OPAC model.

## 1 Introduction

Atmospheric aerosols, which are defined as liquid or solid particles suspended in a gas (Seinfeld and Pandis, 2006), are tiny and mostly not visible to our eyes. Nevertheless, they have an immense impact on our health and on our global climate. Aerosols scatter and absorb solar radiation and by doing so, they directly influence the Earth's radiation budget (see, e.g. Trenberth et al., 2009; Schwartz, 1996; Charlson et al., 1991). In





ACPD
13, 8939–8984, 2013



addition, anthropogenic aerosol particles modify cloud properties, causing, e.g. brighter clouds with longer lifetimes and changed precipitation behavior (see, e.g. Lohmann and Leck, 2005; Ramaswamy et al., 2001; Twomey, 1977). The net effect of anthropogenic aerosols on the Earth's climate is cooling, in contrast to the greenhouse gases which are characterized by a warming effect. However, the Intergovernmental Panel on Climate Change (IPCC, 2007) concludes in its last assessment report that the high uncertainty in the net radiative forcing of all main climate agents is mainly dominated by the large uncertainty in the aerosol radiative forcing. This is mainly caused by the high temporal, spatial, and compositional variability of the aerosol and the poorly understood and quantified aerosol effects.

Since aerosol particles can take up water, they can change in size and chemical composition depending on the ambient relative humidity (RH). Therefore, long-term in-situ measurements of aerosol optical and microphysical properties are usually performed at standardized dry conditions to avoid the RH-effect when quantifying and characterizing the main aerosol properties (WMO/GAW, 2003). This is especially important for the aerosol particle light scattering coefficient $\sigma_{sp}(RH\lambda)$ which strongly depends on RH ($\lambda$ denotes the wavelength). These dry measured values significantly differ from the ambient and thus climate relevant ones. The knowledge of this RH effect is therefore of crucial importance for climate forcing calculations (see, e.g. Haywood and Shine, 1995; Pilinis et al., 1995). In addition, it is also needed for the comparison or validation of remote sensing with in-situ measurements (see, e.g. Zieger et al., 2012, 2011; Morgan et al., 2010; Voss et al., 2001; Ferrare et al., 1998).

The key parameter to describe the influence of RH on the aerosol light scattering is the scattering enhancement factor $f(RH,\lambda)$:

$$f(RH,\lambda) = \frac{\sigma_{sp}(RH,\lambda)}{\sigma_{sp}(RH_{dry},\lambda)}, \quad (1)$$

where $\sigma_{sp}(RH,\lambda)$ is the scattering coefficient at a defined RH and wavelength $\lambda$ and $\sigma_{sp}(RH_{dry},\lambda)$ is the corresponding dry scattering coefficient. $f(RH,\lambda)$ will increase with





ACPD
13, 8939–8984, 2013



increasing RH and will usually be ≥ 1, if the particles do not experience significant restructuring when taking up water (Weingartner et al., 1995). It depends on the size and on the chemical composition of the particle, because both parameters determine the scattering properties and its ability to take up water. In the following, $f$(RH) is discussed for $\lambda = 550$ nm wavelength exemplarily, the explicit reference is omitted from now on for simplicity reasons since only a small wavelength dependency was observed at the five sites for the standard nephelometer wavelengths ($f$(RH = 85 %) varied < 5 % for three wavelengths 450, 550, and 700 nm).

Several studies have measured and modeled $f$(RH) for different aerosol types. Marine aerosols generally showed a higher $f$(RH) and decreased with higher anthropogenic influence (see, e.g. Zieger et al., 2010; Fierz-Schmidhauser et al., 2010c; Wang et al., 2007; Carrico et al., 2003, 2000, 1998; Gasso et al., 2000; McInnes et al., 1998). Urban aerosols (see, e.g. Zieger et al., 2011; Yan et al., 2009; McInnes et al., 1998; Fitzgerald et al., 1982), or continental aerosol particles (see, e.g. Zieger et al., 2013, 2012; Fierz-Schmidhauser et al., 2010a; Sheridan et al., 2001) typically show intermediate values, while mineral dust dominated aerosols or pure biomass burning aerosols are characterized by low values of $f$(RH) (see, e.g. Zieger et al., 2012; Fierz-Schmidhauser et al., 2010b; Kotchenruther and Hobbs, 1998).

In this study, we present a comprehensive overview of the scattering enhancement measured at five European sites during the years 2008 and 2009 with a humidified nephelometer (Fierz-Schmidhauser et al., 2010a, see Sect. 3.1) and other aerosol measurements providing additional information. The sites were selected according to the aerosol type typically encountered at the sites ranging from anthropogenic influenced urban or continental aerosol to clean maritime and Arctic aerosol. The results of the different studies are being related to each other (Sect. 6.1) and are compared to a widely used aerosol model (Sect. 6.4). Recommendations based on the measurement results and on comprehensive closure studies (Sects. 6.2 and 6.3) are given at the end of this study (Sect. 7).





ACPD
13, 8939–8984, 2013



## 2 Site description

A short description of the sites is given in this section and the reader is referred to the cited publications for more detailed information.

### 2.1 Jungfraujoch

At the high alpine site Jungfraujoch (JFJ), located in the Swiss Alps (46.55° N, 7.98° E, 3580 m a.s.l.), mainly free tropospheric air masses were sampled in May 2008, which were interrupted by transport events from the European atmospheric boundary layer (Henne et al., 2010) and occasionally even by long-range transported Saharan dust (Collaud Coen et al., 2004). Henne et al. (2010) characterized the JFJ site as being *mainly remote*. The results of this study are described in detail in Fierz-Schmidhauser et al. (2010b).

### 2.2 Ny-Ålesund

At the Zeppelin station in Ny-Ålesund (NYA), located on the island of Spitsbergen (78.92° N, 11.94° E), typical Arctic aerosol was measured from July to October 2008. This period was characterized by very low particle concentrations and distinct sea salt transports to the station, which is located at an altitude of 475 m a.s.l. Very clean conditions dominated here since no local sources or long-range transport phenomena of pollutants (known as Arctic haze) were observed during this time of the year. The results are presented in Zieger et al. (2010).

### 2.3 Mace Head

At the Mace Head (MHD) station in Ireland (53.33° N, 9.91° W, 5 m a.s.l.), mainly marine and for a shorter period polluted air masses were measured in January and February 2009. The station is located on the west coast of Ireland close to the shore of the ocean. Henne et al. (2010) categorized the MHD site as *generally remote* with a low population





ACPD
13, 8939–8984, 2013



influence. A detailed analysis of this field campaign is given in Fierz-Schmidhauser et al. (2010c).

### 2.4 Melpitz

Field measurements were performed at the Central European research station Melpitz (MEL) in Germany (51.53° N, 12.92° E, 86 m a.s.l.), in January and February 2009. MEL is a rural site, which is surrounded by fields, forests and small villages. The next largest city is Leipzig located ≈ 50 km southwest of the site. Mainly anthropogenic influenced air masses with few transported sea salt events were observed. A detailed description of the intensive campaign is given in Zieger et al. (2013).

### 2.5 Cabauw

The Cabauw site (CAB) is located in the Netherlands in a rural area between the cities of Utrecht and Rotterdam (51.97° N, 4.93° W). It is therefore influenced by transported pollution from the European continent, by local sources as well as by the marine environment. Henne et al. (2010) categorized the CAB site as *agglomeration* which is characterized by large pollution burdens. During the measurement period between June and October 2009 the aerosol at CAB showed a high variability in composition. This work is described in Zieger et al. (2011).

## 3 Experimental

### 3.1 Particle light scattering measurements at elevated relative humidity

The particle light scattering coefficient at elevated RH was measured with a humidified nephelometer (WetNeph), which has been developed at the Paul Scherrer Institute (PSI). The WetNeph is described in detail in Fierz-Schmidhauser et al. (2010a) and only a brief description will be given here. The aerosol is directed from the inlet to





ACPD
13, 8939–8984, 2013



a humidification system, which consists of a humidifier, where the particles are exposed to high RH between 85 % and 90 %, and followed by a Nafion dryer, where the particles are dried again to low RH (usually to RH ≈ 50 %). The WetNeph can be operated in a constant elevated RH mode (usually at RH = 85 % inside the nephelometer cell) or in the humidogram mode. In the latter one, the aerosol stream is first exposed to an increasing RH in the humidifier with the dryer being turned off (hydration) until a high RH inside the nephelometer has been reached (usually RH≈ 85 % depending on the flow and surrounding temperature conditions). The aerosol can then be dried back to low RH by keeping the humidifier at maximum RH and the drier now being turned on (dehydration). With this set-up, both branches of the aerosol's hysteresis curve can be characterized. The particle scattering coefficients are then measured in a modified nephelometer (TSI Inc., Model 3563) at three wavelengths ($\lambda$ = 450, 550 and 700 nm). A reference nephelometer is usually operated in parallel at dry conditions (DryNeph). Besides the routine nephelometer calibration with standard gas, the knowledge of the precise RH inside the nephelometer cell is of crucial importance. This is established by an additional dew point mirror within the system and regular calibrations of the different RH-sensors using standard salt solutions. The WetNeph system has additionally been validated using monodisperse salt measurements of ammonium sulfate and sodium chloride and by applying Mie theory (Fierz-Schmidhauser et al., 2010a).

### 3.2 Additional aerosol measurements

A large variety of further aerosol parameters was measured in parallel during all field campaigns. The data was, e.g. needed to describe the physical and chemical properties responsible for the encountered scattering enhancement, to search for other proxies to predict $f$(RH) and were used for relevant closure studies. The particle light absorption coefficient was measured using either a multi-wavelength aethalometer or a single-wavelength multi-angle absorption photometer (MAAP). The particle number size distribution of the fine mode particles (diameter $D < 1$ µm) was either characterized using a scanning mobility particle sizer (SMPS) or a dual mobility particle size





ACPD
13, 8939–8984, 2013



spectrometer (DMPSS), while the coarse mode particles ($D > 1\,\mu m$) were measured using either an aerodynamic particle sizer (APS) or an optical particle size spectrometer (OPSS). The hygroscopic growth factor, defined as the ratio of the particle diameter at high RH to its dry value (see Eq. (2) below), was added to the analysis using measurements of a hygroscopic tandem differential mobility analyzer (H-TDMA). The chemical composition of the particles was characterized using an aerosol mass spectrometer (AMS) or filter measurements. Table 1 gives an overview of the instrumentation employed at the different sites.

Part of these in-situ measured parameters, together with $\sigma_{sp}$(RH), were used to retrieve the particle light extinction coefficient at ambient RH, which were compared to remote sensing measurements of LIDAR instruments (light detection and ranging; see Zieger et al., 2012, 2011) or were compared to the retrieval of MAX-DOAS measurements (multi-axis differential optical absorption spectroscopy; see Zieger et al., 2011). A good agreement between LIDAR and in-situ measurements was found giving further confidence in our findings.

## 4 Modeling *f*(RH)

The scattering enhancement can be modeled using Mie theory (Mie, 1908). Spherical particles, which were homogeneous and internally or externally mixed, have been assumed in our study. The Mie code used here is based on a computer routine developed by Bohren and Huffman (2004). As a required input, the complex refractive index and the particle number size distribution are needed.

The change in particle diameter due to water uptake is usually described with the hygroscopic growth factor $g$(RH), which is defined as

$$g(\mathrm{RH}) = \frac{D_{\mathrm{wet}}(\mathrm{RH})}{D_{\mathrm{dry}}}, \quad (2)$$





ACPD
13, 8939–8984, 2013



where $D_{dry}$ is the dry particle diameter and $D_{wet}$(RH) the diameter at a specific RH. The hygroscopic growth as a function of RH is physically described by the Köhler theory (Köhler, 1936). The RH dependence of Eq. (2) can be parameterized using a one-parameter relationship which has been introduced, e.g. by Petters and Kreidenweis (2007):

$$g(a_w) = \left(1 + \kappa \frac{a_w}{1 - a_w}\right)^{\frac{1}{3}}, \quad (3)$$

where $a_w$ is the water activity, which can be replaced by RH, if the Kelvin effect can be neglected. This simplification is justified for our cases, because the Kelvin term within the Köhler equation is small for large particles ($D > 80$ nm), which are important for light scattering at the wavelengths used here. The parameter $\kappa$ in Eq. (3) captures all solute properties of the particles (Raoult effect) and is a simple measure of the particle's hygroscopicity, assuming spherical particles with individual homogeneous composition.

The change of the size distribution and the refractive index with changing RH (needed for the Mie calculations) can be calculated with the following procedure:

The increase of the particle diameter is determined by multiplying the dry diameter $D_{dry}$ by the (dry) size dependent hygroscopic growth factor $g(\mathrm{RH}, D_{dry})$:

$$D_{wet}(\mathrm{RH}) = g(\mathrm{RH}, D_{dry}) D_{dry}. \quad (4)$$

The particle number size distribution is then calculated as follows:

$$\frac{\mathrm{d}\tilde{N}(D_{wet})}{\mathrm{d}\log D_{wet}} = \frac{\mathrm{d}N(D_{dry})}{\mathrm{d}\log D_{dry}} \frac{D_{wet}}{D_{dry}} \frac{\mathrm{d}D_{dry}}{\mathrm{d}D_{wet}}. \quad (5)$$

The change of the dry refractive index is calculated by applying a volume weighting of the dry refractive index $m_{dry}$ with the refractive index of water $m_{H_2O}$ (Hale and Querry, 1973):

$$m_{wet} = \frac{m_{dry} + m_{H_2O}(g(\mathrm{RH})^3 - 1)}{g(\mathrm{RH})^3}. \quad (6)$$





ACPD
13, 8939–8984, 2013



For high growth factors and high values of RH, the refractive index of the aerosol droplet converges to the one of water. Although several other mixing rules for the refractive index exist, the volume weighted average was found by Nessler et al. (2005b) to be the most suitable one, since the differences were very small between the different methods and the volume weighting formula was the most simple one to use. $m_{\mathrm{wet}}$ and $\frac{\mathrm{d}\tilde{N}(D_{\mathrm{wet}})}{\mathrm{d}\log D_{\mathrm{wet}}}$ are then the input parameters for the Mie code to calculate the aerosol optical parameters at a specific RH and wavelength.

Figure 1 shows $f(\mathrm{RH},\lambda = 589\,\mathrm{nm})$ as an example for different inorganic salts and for a typical organic substance at a fixed RH of 85 %. A monomodal lognormal size distribution with a width of 1.8 was assumed. The refractive indices were taken from Seinfeld and Pandis (2006); Nessler et al. (2005a) and the hygroscopic growth factors were taken from Topping et al. (2005) and Sjogren et al. (2008). It can be seen that both the size and the chemical composition matter when determining the scattering enhancement. The chemical composition is important for the refractive index, and even more important for the actual hygroscopic growth of the particle. Sodium chloride is one of the most hygroscopic salts and therefore shows the largest values of $f(\mathrm{RH})$, e.g. a lognormal distribution of pure NaCl particle with a mode diameter of 100 nm will scatter at 85 % RH approximately eight times more compared to dry conditions. Figure 1 also shows the possibility of compensating effects between size and chemical composition: A small less hygroscopic particle (e.g. $NH_4HSO_4$) can have the same magnitude of $f(\mathrm{RH})$ as a large more hygroscopic particle (e.g. NaCl). The rather large values in Fig. 1 of $f(\mathrm{RH})$ at small diameters have been reproduced with monodisperse salt measurements in Fierz-Schmidhauser et al. (2010a), where they have been used to assure the measurement quality of our instrument (see Sect. 3.1).





ACPD
13, 8939–8984, 2013



## 5 Closure studies

One goal of our work was to calculate and predict the scattering enhancement using auxiliary measurements, like size distribution, hygroscopic growth, and chemical composition and applying Mie calculations. The first task was to check for consistency within the in-situ measurements, so called closure studies, and in a next step to search for other independently measured parameters that can be used to predict $f$(RH). If the auxiliary aerosol measurements are operated on a continuous basis, e.g. within a monitoring program, they can possibly be used to predict $f$(RH) without explicit RH-dependent optical measurements using, e.g. a humidified nephelometer. Unfortunately, the available suite of aerosol instruments was not identical within the five field campaigns. An overview of the main measurements, the instrument abbreviations and campaign time frames can be found in Table 1. The optical parameters (scattering coefficient at defined RH and at dry conditions as well as the absorption coefficient) were almost completely measured at all sites, while the applied aerosol in-situ techniques varied from site to site. At JFJ, a comprehensive set of instruments were operated. In particular, the bulk aerosol chemical composition was determined with an AMS. The AMS measurements were used to calculate (a) the hygroscopic growth factor (in addition to the direct measurement of the H-TDMA) and (b) the refractive index which is needed as an input parameter for the Mie calculations. At NYA, the chemical composition was only partly determined by filter measurements (which were limited to inorganic substances). Also the hygroscopic growth factor was not measured directly using, e.g. a H-TDMA, instead it was retrieved by Mie theory through an inverse calculation using the measured size distribution, the optical measurements, and an assumption on the refractive index. At MHD, all relevant aerosol measurements except of chemical measurements were available during the observation period. MEL offered detailed chemical composition measurements with an AMS and filter measurements during the entire two months' campaign. The hygroscopic growth measurements using the H-TDMA were only partly available. At CAB, no chemical measurements at all





ACPD
13, 8939–8984, 2013



were available during the observation period, but a H-TDMA was partly deployed. For the closure studies, the SMPS or DMPSS is probably the most important instrument since it measures in the optically relevant size range the particle number concentration usually up to ~550–800 nm with a high precision. It was in operation at all five sites (unfortunately at CAB only for two weeks within the four month's campaign).

## 6 Results

### 6.1 Comparison of the different measurement sites

The measured scattering enhancement factor $f(\mathrm{RH})$ showed individual characteristics significant for each of the five sites. Figure 2 shows FLEXTRA trajectories (Stohl et al., 1995; Stohl and Seibert, 1998) for each site color coded by the $f(\mathrm{RH}=85\,\%)$ value measured at the time of the air parcel arriving at the site. Only periods with available WetNeph measurements are shown. The mean, standard deviation and percentile values of $f(\mathrm{RH}=85\,\%)$ are given in Table 2.

For JFJ, Fig. 2 reveals that the air masses were mainly originating from Central Europe but also had their origin in the North African regions. These air masses transported mineral dust particles as well up to JFJ. Since mineral dust shows low hygroscopic growth, their $f(\mathrm{RH}=85\,\%)$ values are low compared to other air masses.

At CAB, air masses with low $f(\mathrm{RH}=85\,\%)$ values mainly had their origin in the industrialized areas of, e.g. the Ruhr area, Northern France, Southern Britain, the Netherlands, and Belgium. $f(\mathrm{RH}=85\,\%)$ was elevated at CAB when the air masses originated from the Atlantic Ocean or the Northern Sea and contained hygroscopic sea salt. However, only few clear sea salt events were observed at CAB, e.g. showing hysteresis behavior as one would expect from pure inorganic salts like NaCl.

The clean and polluted sectors can be identified at MHD: $f(\mathrm{RH})$ was generally higher when air masses arrived from the sea (mean $f(\mathrm{RH}=85\,\%)=2.28$), while the air masses from the polluted eastern sector, which had contact with the urban areas of





ACPD
13, 8939–8984, 2013



Ireland and the UK, were characterized with smaller values (mean $f(\mathrm{RH}=85\,\%)=1.8$). The maritime air masses with dominating sea salt were also seen in the hysteresis behavior of the recorded humidograms.

MEL showed generally larger values of $f(\mathrm{RH})$ (mean $f(\mathrm{RH}=85\,\%)=2.77$), with air masses originating mainly from the western and northwestern part of Europe. No distinct sectors could be identified during the observation period in winter 2009. Sea salt with coincident hysteresis in the humidograms was observed at MEL.

As an extreme, the NYA site showed the largest $f(\mathrm{RH}=85\,\%)$ compared to the other sites which could range up to values of 6.6. The main catchment area at NYA was the open oceans and ice shields of the Arctic, bringing, e.g. clean sea salt to the site. The mean values for non-sea salt influenced periods were higher (mean $f(\mathrm{RH}=85\,\%)=3.41$) than the sea salt periods (mean $f(\mathrm{RH}=85\,\%)=2.86$). This was attributed to compensation effects of size and hygroscopicity: Smaller and less hygroscopic particles can have similar (or even larger) values of $f(\mathrm{RH})$ than larger and more hygroscopic particles (see Fig. 1).

The $f(\mathrm{RH}=85\,\%)$-values measured at all five sites are shown as probability density functions (PDF) in Fig. 3. The two-sector discrimination of MHD can be clearly seen. JFJ, MEL and MHD show similar values of $f(\mathrm{RH}=85\,\%)$, while MEL and especially NYA are characterized with generally larger values. The larger values at NYA can be explained by the absence of anthropogenic influence and the size and hygroscopicity of the particles.

Example humidograms of $f(\mathrm{RH})$ measured at the five sites are depicted in Fig. 4. The color code is related to the anthropogenic influence (bluish curves: more clean conditions with higher amount of sea salt; reddish curves: more anthropogenic influences or mineral dust episodes (JFJ). These average humidograms show the high variability in curve shape, hysteresis behavior and magnitude. The individual humidograms will be separately shown again in Sect. 6.4 (Figs. 9 and 10) with a comparison to model data.





ACPD
13, 8939–8984, 2013



## 6.2 Closure studies

As mentioned above, all closure studies had their individual settings due to the site-specific availability of auxiliary aerosol measurements and different instrumentations (see Table 1). Figure 5 shows the ratio of the predicted to measured value of $f(\mathrm{RH})$ as probability density functions for the five sites. An optical closure was achieved at all five sites, giving again confidence in the performed in-situ measurements of $f(\mathrm{RH})$.

At JFJ, the best closure was achieved, if the measured size distribution, the chemical composition (refractive index) and the hygroscopic growth factor (AMS or H-TDMA) were used in the Mie model. The slightly higher predicted values were probably due to calibration issues of the RH sensor inside the WetNeph. Keeping the chemical composition constant (refractive index and hygroscopic growth) or the size distribution shape constant still delivered reasonable prediction results, showing that a mean chemical composition is sufficient to predict $f(\mathrm{RH})$. This result is in accordance with findings of Jurányi et al. (2010) who showed that for a prediction of the cloud condensation nuclei (CCN) number concentration, using measured size distribution and hygroscopicity measurements (H-TDMA), a mean chemical composition is sufficient. Nessler et al. (2005a) proposed a very simplified scheme to predict $f(\mathrm{RH})$ for the summer and winter periods separately, using the measured Ångström exponent of the dry scattering coefficient. A systematic overestimation with a slightly broader distribution of the PDF of the predicted to measured value of $f(\mathrm{RH}=85\,\%)$ is observed due to the simplifications in this model (see orange curve in Fig. 5a). This model is based on the fact that the aerosol coarse mode at JFJ consists mainly of non-hygroscopic mineral dust which is characterized by low Ångström exponents, in contrast to the other four sites where the coarse mode was mainly attributed to sea salt. However, a full seasonal validation of the model by Nessler et al. (2005a) would be desirable.

At NYA, the measured values of $f(\mathrm{RH}=85\,\%)$ were in general higher compared to the other sites (see Fig. 3). The full chemical composition and the hygroscopic growth were not measured directly. Nevertheless, the hygroscopic growth was retrieved from





ACPD
13, 8939–8984, 2013



the measured size distribution, and the absorption and scattering properties using again Mie theory. As summarized in Fig. 5b, also a mean hygroscopicity (using a growth factor of $g(\mathrm{RH}=85\,\%)=1.6$) is sufficient to predict $f(\mathrm{RH}=85\,\%)$ at NYA, although with a higher uncertainty compared to JFJ. Although a mean $g(\mathrm{RH})$ was partially sufficient for the prediction, it can also lead to large uncertainties in the predicted $f(\mathrm{RH})$, as can be seen in Fig. 5b, where the upper and lower bound of the retrieved $g(\mathrm{RH})$ was used as a constant value for the entire time series. A parameterization of $g(\mathrm{RH})$ using the measured volume coarse mode fraction only brought a slight improvement in Zieger et al. (2010).

At MHD (Fig. 5c), the calculations were performed assuming a different refractive index for the polluted (higher imaginary part) and clean sector separately (Fierz-Schmidhauser et al., 2010c). The $g(\mathrm{RH})$ of the H-TDMA was only available at $D_{\mathrm{dry}}=165\,\mathrm{nm}$. The closure was achieved for both cases. For the clean case, the agreement was slightly worse, which was attributed to the assumption of the refractive index and problems in combining the two size distribution measurements of coarse and fine mode, which showed discrepancies when comparing the surface size distribution.

For CAB, the situation is more complex, because the aerosol origin showed larger fluctuations. Besides the continental and urban influence, the close by marine environment also contributed to the aerosol composition. As described in Zieger et al. (2011), the measured hygroscopic growth factor is limited to smaller size ranges since the largest dry diameter of the deployed H-TDMA was 165 nm. The larger particles in the coarse mode were therefore missed by the H-TDMA. Since the coarse mode can be influenced by highly hygroscopic sea salt particles, the ratio of predicted to measured values of $f(\mathrm{RH}=85\,\%)$ in Fig. 5d (blue curve) using the growth factor $g(\mathrm{RH})$ of the H-TDMA is shifted towards an underestimation of the predicted $f(\mathrm{RH}=85\,\%)$. A proposed parameterization of $g(\mathrm{RH})$ using the coarse mode volume fraction and black carbon (BC) volume fraction improved the agreement to the measured values. Assuming a constant value of $g(\mathrm{RH})$, which can be done for JFJ and NYA, is not sufficient at CAB as can be seen in Fig. 5d (green curve).





ACPD
13, 8939–8984, 2013



Closure was also achieved at MEL (Fig. 5e). The best result was achieved if the refractive index and growth factor was derived from the AMS (plus MAAP) measurements. Both instruments were operated successfully during the entire campaign, while the H-TDMA was only partly available. A mean $g(\mathrm{RH} = 90\,\%) = 1.53$ was found to be sufficient for the prediction at MEL, however with exceptions especially during transported sea salt and high anthropogenic pollution events. In addition, the coarse mode composition was varied for the calculation: If a very hygroscopic coarse mode of NaCl was assumed, the $f(\mathrm{RH})$ was clearly overpredicted, while an assumed dust coarse mode clearly leads to an underprediction of $f(\mathrm{RH})$.

In summary, both size and chemical composition mattered when determining $f(\mathrm{RH})$, which is schematically depicted in Fig. 6. For the aerosol discussed here, the relative contributions of the accumulation to the coarse mode and the specific chemical composition were important. At JFJ, the coarse mode was most probably attributed to long-range transported non-hygroscopic mineral dust, whereas at NYA, MEL, MHD, and CAB it was also dominated by hygroscopic sea salt. Sea salt was never observed at JFJ which also explains the absence of hysteresis effects (which was occasionally observed at all other sites). The accumulation mode was dominated either by organic substances with low hygroscopicity, non-hygroscopic BC, or by hygroscopic inorganic salts. As seen in Fig. 1, the interaction between size and hygroscopicity can lead to compensation effects for $f(\mathrm{RH})$, as observed at NYA, where smaller and less hygroscopic particles had the same magnitude of $f(\mathrm{RH})$ as larger and more hygroscopic particles (Zieger et al., 2010).

### 6.3 Can a simple recipe be established for the $f(\mathrm{RH})$-prediction?

To show the difficulty in retrieving a simple recipe for an accurate $f(\mathrm{RH})$-prediction, we have performed Mie calculations varying the main input parameters in the typical





ACPD
13, 8939–8984, 2013



encountered ranges. A bimodal lognormal size distribution was assumed

$$\frac{\mathrm{d}N_i(D)}{\mathrm{d}\log D} = \frac{N_i}{\sqrt{2\pi}\log\sigma_i}\exp\left[-\frac{1}{2}\left(\frac{\log D - \log D_{\mathrm{mod},i}}{\log\sigma_i}\right)^2\right], \quad (7)$$

where $D$ denotes the diameter, $D_{\mathrm{mod},i}$ the mode diameter, $N_i$ the total particle number density, and $\sigma_i$ the width (or standard deviation) of the distribution of mode $i$ (with $i = 1$ as the fine mode (FM) and $i = 2$ as the coarse mode (CM)).

The following parameters were varied:

- Fine mode diameter ($D^{\mathrm{FM}}_{\mathrm{mod}}$)
- Coarse mode number fraction (CM frac = $N_{\mathrm{CM}}/(N_{\mathrm{FM}} + N_{\mathrm{CM}})$)
- Fine mode hygroscopicity ($\kappa_{\mathrm{FM}}$, see Eq. 3)
- Coarse mode hygroscopicity ($\kappa_{\mathrm{CM}}$)
- Width of fine mode ($\sigma$)
- Imaginary part of refractive index ($m_{\mathrm{imag}}$)

The coarse mode diameter was assumed to be constant at $D = 2\,\mu\mathrm{m}$. The real part of the refractive index was assumed to be $m = 1.54$, while the calculations were performed for $\lambda = 550\,\mathrm{nm}$ and RH = 85 %.

The result for a constant refractive index and a width of $\sigma = 1.8$ for coarse and fine mode is depicted in Fig. 7 for four different coarse mode number fractions (CM frac = 0.02, 0.01, 0.00001, 0) and alternating for a very hygroscopic ($\kappa = 1$) or non-hygroscopic ($\kappa = 0$) coarse or fine mode. The dominance even of small amounts of the coarse mode particles in the overall $f$(RH) can be seen. The coarse mode can suppress the $f$(RH) in case of dust particles or enhance the overall $f$(RH) in case of very hygroscopic particles (e.g. pure NaCl). The mode diameter determines if the mode at enhanced RH (here 85 %) is moving into the optically relevant size range. This separate growing into the





ACPD
13, 8939–8984, 2013



optical active size range also explains the wave-like structures seen in Fig. 7. Under the full absence of coarse mode particles, the $f$(RH)-values can reach higher values and the shapes (as a function of the fine mode diameter) are similar to the calculation of the monodisperse substances shown in Fig. 1.

Figure 8 shows the dependence of $f$(RH) on the mode width ($\sigma$) of the fine mode and the imaginary part, again for different coarse mode number fractions and for a highly hygroscopic or non-hygroscopic coarse mode (sea salt or dust, respectively) as the two extremes. The dependence of $f$(RH) with respect to a varying $\sigma$ or imaginary part of $m$ is less pronounced than the parameters discussed above. The strong influence of the coarse mode number fraction is seen in a similar way as in Fig. 7.

This exercise demonstrates a high dependency of $f$(RH) on the different size and hygroscopicity parameters. It also shows that a simple recipe of $f$(RH) for all important aerosol types can not be achieved without the knowledge of further constraints like the mean fine mode diameter or the composition of the coarse mode. For sites with low variation of the aerosol microphysical properties, a site specific proxy can be used to predict $f$(RH), while the same proxy would fail for another site. As an example, at JFJ, the Ångström exponent of particle scattering coefficient (as a proxy for the mean size) can be used to estimate $f$(RH) (Nessler et al., 2005a). This proxy is only applicable, because the coarse mode at JFJ predominantly consists of (non-hygroscopic) mineral dust, while the same proxy will fail for sites with sea salt influence, where the coarse mode will be dominated by hygroscopic substances. A reliable prediction of $f$(RH) will therefore always need a full determination of the particle number distribution (fine and coarse mode) and an information on the hygroscopicity and/or main chemical composition.

### 6.4 Comparison to OPAC

The measured scattering enhancement factors were compared to the database OPAC (optical properties of aerosol and clouds) by Hess et al. (1998). OPAC is a popular database on aerosol and cloud optical properties, which is widely used in the scientific





ACPD
13, 8939–8984, 2013



community[1] since it provides a comprehensive set of microphysical and optical data of aerosols and clouds. It is closely linked to the Global Aerosol Data Set (GADS) by Köpke et al. (1997). The data is stored as components that are meant to be representative for a certain origin (Hess et al., 1998). All components represent average conditions and the authors clearly state that the given values may not necessarily be valid for actual conditions. Nevertheless, a comparison of the measurements performed here to OPAC is a needed scientific task as a first step to improve future versions of OPAC.

The main OPAC aerosol components will be briefly described here in the following. The *water-soluble* component combines all aerosol particles that originate from gas to particle conversion (including various kinds of sulfates, nitrates, and also organic substances), while the *insoluble* component describes soil particles which also contain organic compounds, but do not experience hygroscopic growth. The *soot* component describes the absorbing black carbon. The *sea salt* components are given for the accumulation and the coarse mode separately and both are dependent on RH. To describe desert originated aerosols, different *mineral* components are provided. A special *mineral-transported* component is used to describe long-range transported mineral dust. The *sulfate* component is mainly used to describe the highly sulfate containing Antarctic aerosol and is also used to model the stratospheric background aerosol. It is composed of 75 % $H_2SO_4$ and is able to take up water and therefore depends on RH.

Besides the wavelength dependent refractive index, the number size distribution of each component is provided as a lognormal size distribution (see Eq. 7). The size parameters and refractive indexes are provided for eight different RH's (0 %, 50 %, 70 %, 80 %, 90 %, 95 %, 98 %, and 99 %) for the RH-dependent components. The OPAC components can be externally mixed (using the number mixing ratio of each component) to different aerosol types. Hess et al. (1998) propose aerosol types (ready mixtures) as examples that are typically found in the atmosphere.

[1] *ISI Web of Knowledge* lists over 881 citations (last access: 8 March 2013).





ACPD
13, 8939–8984, 2013



The strength of OPAC is the option to individually compose aerosol types (using the number mixing ratio, as mentioned above). Therefore, our measurements will also be compared to individually mixed aerosol types besides the aerosol examples that are proposed in OPAC. These mixtures were calculated when full size distribution measurements were available at the same time. The number mixing ratio $n_i$ for each component was calculated as follows:

$$n_i = \frac{N_i}{N_{\text{tot}}} = \left( \int_{D_{i,\text{min}}}^{D_{i,\text{max}}} \frac{\mathrm{d}N(D)}{\mathrm{d}\log D} \mathrm{d}\log D \right) \Big/ N_{\text{tot}}, \tag{8}$$

where $N_i$ is the number concentration between $D_{i,\text{min}}$ and $D_{i,\text{max}}$, which is determined by taking the middle value of $D$ between the individual mode diameters of two neighboring components, and $N_{\text{tot}}$ is the total number concentration. For a mixture of *water-soluble* and *sea salt (acc. mode)* components for example, the size distribution would be integrated from 0 to 187.8 nm to calculate the apparent number concentration of the *water-soluble* component and from 187.8 nm to the end of the measured distribution for the number concentration of the *sea salt (acc. mode)* component. For CAB, the mixture was composed taking the *soot*, the *water-soluble*, and the two *sea salt* components. For NYA, the *water-soluble* and the two *sea salt* components were chosen, while for JFJ only the *water-soluble* and the *mineral-transported* components were taken for the calculation of $f$(RH).

Figures 9 and 10 show example humidograms recorded at the five sites (grey points) compared to the OPAC example aerosol types, which would have been expected to be observed at the specific site. The individually mixed OPAC results are shown (called *OPAC mix* in Figs. 9 and 10) for time periods when corresponding size distribution measurements were available. For the same periods, the result of the Mie model calculations has been added (magenta line in Figs. 9 and 10), which used the measured (or for NYA retrieved) $\kappa$-value (see Eq. 3) and the measured particle number size distribution





ACPD
13, 8939–8984, 2013



as input. Humidograms without a magenta curve in Figs. 9 and 10) therefore had no parallel hygroscopicity or particle number size distribution measurements.

In general, Figs. 9 and 10 reveal that the calculated values using the OPAC input data, which are only given for eight discrete RH values, are clearly higher than the measured values of $f$(RH) for all five sites, except for the Saharan dust event at JFJ, which is well described by OPAC (see Fig. 10i). OPAC is not capable to describe hysteresis effects observed, e.g. for clean maritime air (see Fig. 9a and g) and only refers to the deliquesced state (same as for the $\kappa$-equation).

The shape also significantly differs from the measurements, especially for low and medium values of RH. Taking the measured number size distribution with re-mixed OPAC components does not improve the agreement significantly, except for the CAB maritime slightly polluted case (Fig. 9d). The calculated $f$(RH) curve using the measured (or retrieved) $\kappa$-value seems to perform well, indicating that the $\kappa$-equation (Eq. 3) is suitable to describe the curvature of $f$(RH) in combination with Mie calculations.

The overestimation by OPAC could be explained by:

a. the implemented hygroscopic growth

b. the fixed size distribution modes

c. the used refractive indices

of the individual components. The influence of the refractive index can not be checked due to missing chemical composition measurements, while the influence of the implemented size distributions and the hygroscopic growth can be tested against the measurements where available (see below).

The *water-soluble* and *soot* components are the two main components to describe the fine mode in OPAC besides the *sea salt (acc. mode)*. The OPAC aerosol type surface size distributions are compared to the measured ones in Fig. 11a–f. The number size distributions have been transferred to (normalized) surface size distributions, since





ACPD
13, 8939–8984, 2013



they are a better representation for the optically relevant size ranges. For the proposed aerosol type examples, the surface size distributions are mainly shifted to smaller diameters and are also characterized by larger mode widths compared to the measured distributions. The concentration (or particle surface) is as well different to the measurements. Mixing the components according to the measured number size distribution (using Eq. (8), as described above) does not improve the comparison, since the fixed distribution modes and widths make an accurate mixing difficult (see magenta line in Fig. 11a–f).

The hygroscopic growth factor $g$(RH) in OPAC is based according to Hess et al. (1998) on the work of Hänel and Zankl (1979) and is shown in Fig. 12 for the four RH-dependent OPAC components (red bullets). However, they differ from the original data of Hänel and Zankl (1979) (R. Dlugi, personal communication, March 2013, which are shown as blue crosses in Fig. 12). Therefore, a possible erroneous implementation of the hygroscopic growth within OPAC could be a major reason of the found differences. In addition, Fig. 12 shows the $g$(RH) calculated using the $\kappa$-equation (see Eq. 3). For the *sea salt* components $g(\mathrm{RH} = 90\,\%) = 2.1$ was taken from Swietlicki et al. (2008) for highly hygroscopic marine aerosol. For the *water-soluble* component a mean value of $g(\mathrm{RH} = 90\,\%) = 1.48$ measured by the H-TDMA during the Cabauw campaign was taken, while for the *sulfate droplets* $g(\mathrm{RH} = 90\,\%) = 2.05$ was taken from Topping et al. (2005). The implemented hygroscopic growth in OPAC is not in correspondence with the course of $g$(RH) if the $\kappa$-equation is taken into account. Especially for low RH ($< 80\,\%$) the OPAC values are clearly above the $\kappa$-curve, while for higher RH the agreement seems to be better. As shown in the example humidograms (see Figs. 9 and 10), the $\kappa$-equation is a good approximation to describe the hygroscopic growth in terms of $f$(RH) at different RH in combination with the measured size distribution, an appropriate refractive index, and Mie theory. However, it is not suitable to describe the hysteresis effect of aerosol humidification.

To further investigate the influence of the hygroscopic growth as implemented in OPAC, the hygroscopic growth of the *water-soluble* and *sea salt (acc. and*





ACPD
13, 8939–8984, 2013



*coarse mode)* was modified and tested against measurements at CAB, where the most reliable $g$(RH)-measurements were obtained. For the modification part, the hygroscopic growth of the *water-soluble* and the *sea salt (acc. and coarse mode)* components was changed. The mean $g(\mathrm{RH} = 90\,\%) = 1.48$ measured during the CAB campaign at 165 nm was taken for the *water-soluble* component, and $g(\mathrm{RH} = 90\,\%) = 2.1$ was taken for the two *sea salt* components from Swietlicki et al. (2008). Again, the $\kappa$-equation was taken to calculate $g$(RH) at different RH values (see violet curve in Fig. 12a-c for the applied growth factors). The time period of the closure study during the CAB campaign was chosen (4–18 July 2009), which is considered to be the most complete time series covering a wide range of different aerosol types, ranging from continental to maritime aerosol types. The number mixing ratios (or number concentrations) of both modes were again calculated using Eq. (8). The *soot*, *water-soluble*, and *sea salt (acc. mode and coarse mode)* components were found to be the most dominant components during the period of the CAB closure study.

Taking the original components *soot*, *water-soluble*, and *sea salt (acc. and coarse mode)*, OPAC overestimates $f$(RH) especially for the low and medium RH values, as already seen in the example humidograms in Figs. 9 and 10 and as shown in Fig. 13a, where the ratio of calculated to measured value is seen for the above mentioned closure period at CAB. It improves towards higher RH, but the ratio is still above 1 at 90 % RH. Modifying the *water-soluble* and *sea salt (acc. and coarse mode)* components leads to an improved agreement between calculated and observed $f$(RH) (see Fig. 13b). The remaining discrepancy is probably caused by the fixed distribution modes and in general by the simplification of the aerosol at CAB when assuming only four main components.

## 7 Recommendations

The following recommendations concerning a precise measurement and prediction of $f$(RH) can be derived from this study:





ACPD
13, 8939–8984, 2013



- For a precise measurement of $f$(RH), a humidified nephelometer should be used. A crucial point is a good temperature control and the knowledge of the exact RH inside the nephelometer cell. The RH-sensors and the entire system should therefore be calibrated using standard salt solutions and monodisperse salt measurements and Mie theory (Fierz-Schmidhauser et al., 2010a).
- If no direct measurements of $f$(RH) are available, $f$(RH) can be approximated using the measured particle number size distribution, the hygroscopic growth factor and chemical composition measurements and Mie theory. The $\kappa$-equation (Eq. 3) should be used to describe the RH-dependency of $g$(RH).
- The hygroscopic growth measurements with a standard H-TDMA may miss the important coarse mode contribution to $f$(RH) and therefore may under- or overestimate the overall $f$(RH) (see Figs. 7 and 8 but also Fig. 6 in Zieger et al., 2011).
- The humidogram measurements of $f$(RH) allow to identify hysteresis behavior and can be used to further identify air mass origin (e.g. sea salt).
- Optical closure studies may help to identify measurement errors and model weaknesses. They are useful to constrain the obtained measurement results.
- The hygroscopic growth within the OPAC (Hess et al., 1998) components should be replaced by current literature values. For the two *sea salt* components, we propose $g$(RH = 90 %) = 2.1, $g$(RH = 90 %) = 1.48 for the *water-soluble* component, and $g$(RH = 90 %) = 2.02 for the *sulfate droplets* component. The RH-dependency of $g$(RH) can be approximated for the upper branch using the $\kappa$-equation (Eq. 3).

## 8 Conclusions

The effect of hygroscopic growth on aerosol particle light scattering has been investigated at five European sites using measurements and model calculations. Each site





ACPD
13, 8939–8984, 2013



has been chosen to be representative for a certain aerosol type. A high spatial and temporal variability of $f$(RH) has been observed throughout Europe, starting from low values of long-range transported mineral dust to intermediate values for continental aerosol to high values for pristine maritime or Arctic aerosol. Hysteresis was observed when pure sea salt was present. Compensating effects between size and hygroscopicity were observed in the Arctic. The increase in variability and complexity in aerosol composition increased from remote sites to urban and continental sites, and therefore the number of known parameters needed to predict of $f$(RH) increased concurrently. Free tropospheric aerosol found, e.g. at the Jungfraujoch can be simply parameterized using the Ångström exponent (Nessler et al., 2005b). This rather simplistic approach can only be made at this site due to that fact that increased coarse mode fractions (low Ångström exponents) at the Jungfraujoch will most likely be a proxy for more mineral dust with reduced hygroscopicity and therefore result in a lower $f$(RH). For the other sites, an enlarged coarse mode points to an enlarged sea salt contribution, which in contrast to mineral dust is highly hygroscopic. Therefore, a simple proxy like the Ångström exponent as a proxy for size can not be used alone to predict $f$(RH) for other sites. Instead, information on the full size distribution is needed. For example, for the Arctic aerosol found in summer and fall in Ny-Ålesund in the Arctic a single hygroscopicity ($\kappa$-value) and measured size distribution together with a Mie model were found to be sufficient to calculate the ambient value of the scattering coefficient. The high variability of aerosol composition and size at Cabauw made a precise prediction of the scattering enhancement difficult. Here, only measurements of the full size distribution and the full size resolved chemical composition will make a good prediction of $f$(RH) possible, if no explicit humidified nephelometer measurements are available. A comparison to the OPAC dataset (Hess et al., 1998) showed a systematic overprediction of $f$(RH) especially at intermediate RH. The bias can be reduced, if the implemented hygroscopic growth within OPAC is replaced by current literature values given here.





ACPD
13, 8939–8984, 2013



*Acknowledgements.* We thank all collaborators and co-authors of the related individual studies. Ralph Dlughi is acknowledged for providing the original data of Hänel and Zankl (1979). We thank the Norwegian Institute for Air Research (NILU) for providing the FLEXTRA trajectory calculations. This work was financially supported by the EC-projects European Supersites for Atmospheric Aerosol Research (EUSAAR, contract 026140), Aerosols, Clouds, and Trace gases Research Infrastructure Network (ACTRIS, contract 262254) and Global Earth Observation and Monitoring (GEOMON, contract 026140), by MeteoSwiss in the framework of the Global Atmosphere Watch Program, as well as by the European Space Agency's Climate Change Initiative (aerosol_cci).

## References

Bohren, C. and Huffman, D.: Absorption and Scattering of Light by Small Particles, Wiley-VCH, Weinheim, 2004. 8946

Carrico, C., Rood, M., and Ogren, J.: Aerosol light scattering properties at Cape Grim, Tasmania, during the first Aerosol Characterization Experiment (ACE 1), J. Geophys. Res., 103, 16565–16574, doi:10.1029/98JD00685, 1998. 8942

Carrico, C., Rood, M., Ogren, J., Neusüß, C., Wiedensohler, A., and Heintzenberg, J.: Aerosol optical properties at Sagres, Portugal, during ACE-2, Tellus B, 52, 694–715, doi:10.1034/j.1600-0889.2000.00049.x, 2000. 8942

Carrico, C., Kus, P., Rood, M., Quinn, P., and Bates, T.: Mixtures of pollution, dust, sea salt, and volcanic aerosol during ACE-Asia: radiative properties as a function of relative humidity, J. Geophys. Res., 108, 8650, doi:10.1029/2003JD003405, 2003. 8942

Charlson, R., Langner, J., Rodhe, H., Leovy, C., and Warren, S.: Perturbation of the Northern Hemisphere radiative balance by backscattering from anthropogenic sulfate aerosols, Tellus A, 43, 152–163, 1991. 8940

Collaud Coen, M., Weingartner, E., Schaub, D., Hueglin, C., Corrigan, C., Henning, S., Schwikowski, M., and Baltensperger, U.: Saharan dust events at the Jungfraujoch: detection by wavelength dependence of the single scattering albedo and first climatology analysis, Atmos. Chem. Phys., 4, 2465–2480, doi:10.5194/acp-4-2465-2004, 2004. 8943





ACPD

13, 8939–8984, 2013



Ferrare, R., Melfi, S., Whiteman, D., Evans, K., and Leifer, R.: Raman lidar measurements of aerosol extinction and backscattering 1. Methods and comparisons, J. Geophys. Res., 103, 19663–19672, doi:10.1029/98JD01646, 1998. 8941

Fierz-Schmidhauser, R., Zieger, P., Wehrle, G., Jefferson, A., Ogren, J. A., Baltensperger, U., and Weingartner, E.: Measurement of relative humidity dependent light scattering of aerosols, Atmos. Meas. Tech., 3, 39–50, doi:10.5194/amt-3-39-2010, 2010a. 8942, 8944, 8945, 8948, 8962

Fierz-Schmidhauser, R., Zieger, P., Gysel, M., Kammermann, L., DeCarlo, P. F., Baltensperger, U., and Weingartner, E.: Measured and predicted aerosol light scattering enhancement factors at the high alpine site Jungfraujoch, Atmos. Chem. Phys., 10, 2319-2333, doi:10.5194/acp-10-2319-2010, 2010b. 8942, 8943, 8970

Fierz-Schmidhauser, R., Zieger, P., Vaishya, A., Monahan, C., Bialek, J., O'Dowd, C. D., Jennings, S. G., Baltensperger, U., and Weingartner, E.: Light scattering enhancement factors in the marine boundary layer (Mace Head, Ireland), J. Geophys. Res., 115, D20204, doi:10.1029/2009jd013755, 2010c. 8942, 8944, 8953, 8970

Fitzgerald, J., Hoppel, W., and Vietti, M.: The size and scattering coefficient of urban aerosol particles at Washington, DC as a function of relative humidity, J. Atmos. Sci., 39, 1838–1852, 1982. 8942

Gasso, S., Hegg, D., Covert, D., Collins, D., Noone, K., Öström, E., Schmid, B., Russell, P., Livingston, J., Durkee, P., and Jonsson, H.: Influence of humidity on the aerosol scattering coefficient and its effect on the upwelling radiance during ACE-2, Tellus B, 52, 546–567, 2000. 8942

Hale, G. and Querry, M.: Optical constants of water in the 200-nm to 200-µm wavelength region, Appl. Optics, 12, 555–563, doi:10.1364/AO.12.000555, 1973. 8947

Hänel, G. and Zankl, B.: Aerosol size and relative humidity: water uptake by mixtures of salts, Tellus, 31, 478–486, doi:10.1111/j.2153-3490.1979.tb00929.x, 1979. 8960, 8964, 8983

Haywood, J. and Shine, K.: The effect of anthropogenic sulfate and soot aerosol on the clear sky planetary radiation budget, Geophys. Res. Lett., 22, 603–606, doi:10.1029/95GL00075, 1995. 8941

Henne, S., Brunner, D., Folini, D., Solberg, S., Klausen, J., and Buchmann, B.: Assessment of parameters describing representativeness of air quality in-situ measurement sites, Atmos. Chem. Phys., 10, 3561–3581, doi:10.5194/acp-10-3561-2010, 2010. 8943, 8944





ACPD
13, 8939–8984, 2013



Hess, M., Koepke, P., and Schult, I.: Optical properties of aerosols and clouds: the software package OPAC, Bull. Amer. Meteor. Soc., 79, 831–844, 1998. 8940, 8956, 8957, 8960, 8962, 8963, 8980

IPCC: Climate Change 2007: The Physical Science Basis. Contribution of Working Group I to the Fourth Assessment Report of the Intergovernmental Panel on Climate Change, Cambridge University Press, 2007. 8941

Jurányi, Z., Gysel, M., Weingartner, E., DeCarlo, P. F., Kammermann, L., and Baltensperger, U.: Measured and modelled cloud condensation nuclei number concentration at the high alpine site Jungfraujoch, Atmos. Chem. Phys., 10, 7891–7906, doi:10.5194/acp-10-7891-2010, 2010. 8952

Köhler, H.: The nucleus in and the growth of hygroscopic droplets, Transactions of the Faraday Society, 32, 1152–1161, 1936. 8947

Köpke, P., Hess, M., Schult, I., and Shettle, E.: Global Aerosol Data Set, Report No. 243, Max-Planck-Institut für Meteorologie, 1997. 8957

Kotchenruther, R. and Hobbs, P.: Humidification factors of aerosols from biomass burning in Brazil, J. Geophys. Res., 103, 32081–32089, doi:10.1029/98JD00340, 1998. 8942

Lohmann, U. and Leck, C.: Importance of submicron surface-active organic aerosols for pristine Arctic clouds, Tellus B, 57, 261–268, 2005. 8941

McInnes, L., Bergin, M., Ogren, J., and Schwartz, S.: Apportionment of light scattering and hygroscopic growth to aerosol composition, Geophys. Res. Lett., 25, 513–516, doi:10.1029/98GL00127, 1998. 8942

Mie, G.: Beiträge zur Optik trüber Medien, speziell kolloidalen Metalllösungen, Ann. Phys., 25, 377–445, 1908. 8946

Morgan, W. T., Allan, J. D., Bower, K. N., Esselborn, M., Harris, B., Henzing, J. S., Highwood, E. J., Kiendler-Scharr, A., McMeeking, G. R., Mensah, A. A., Northway, M. J., Osborne, S., Williams, P. I., Krejci, R., and Coe, H.: Enhancement of the aerosol direct radiative effect by semi-volatile aerosol components: airborne measurements in North-Western Europe, Atmos. Chem. Phys., 10, 8151–8171, doi:10.5194/acp-10-8151-2010, 2010. 8941

Nessler, R., Weingartner, E., and Baltensperger, U.: Adaptation of dry nephelometer measurements to ambient conditions at the Jungfraujoch, Environ. Sci. Technol., 39, 2219–2228, doi:10.1021/es035450g, 2005a. 8948, 8952, 8956, 8972

Nessler, R., Weingartner, E., and Baltensperger, U.: Effect of humidity on aerosol light absorption and its implications for extinction and the single scattering albedo illustrated for a site in





ACPD
13, 8939–8984, 2013



the lower free troposphere, J. Aerosol Sci., 36, 958–972, doi:10.1016/j.jaerosci.2004.11.012, 2005b. 8948, 8963
Petters, M. D. and Kreidenweis, S. M.: A single parameter representation of hygroscopic growth and cloud condensation nucleus activity, Atmos. Chem. Phys., 7, 1961–1971, doi:10.5194/acp-7-1961-2007, 2007. 8947
Pilinis, C., Pandis, S., and Seinfeld, J.: Sensitivity of direct climate forcing by atmospheric aerosols to aerosol size and composition, J. Geophys. Res., 100, 18739–18754, doi:10.1029/95JD02119, 1995. 8941
Ramaswamy, V., Boucher, O., Haigh, J., Hauglustaine, D., and Haywood, J.: Radiative Forcing of Climate Change, Cambridge University Press, Cambridge, UK and New York, NY, USA, 2001. 8941
Schwartz, S.: The Whitehouse effect–shortwave radiative forcing of climate by anthropogenic aerosols: an overview, J. Aerosol Sci., 27, 359–382, 1996. 8940
Seinfeld, J. and Pandis, S.: Atmospheric Chemistry and Physics: From Air Pollution to Climate Change, John Wiley and Sons, Inc., Hoboken, New Jersey, 2006. 8940, 8948, 8972
Sheridan, P., Delene, D., and Ogren, J.: Four years of continuous surface aerosol measurements from the Department of Energy's Atmospheric Radiation Measurement Program Southern Great Plains Cloud and Radiation Testbed site, J. Geophys. Res., 106, 20735–20747, 2001. 8942
Sjogren, S., Gysel, M., Weingartner, E., Alfarra, M. R., Duplissy, J., Cozic, J., Crosier, J., Coe, H., and Baltensperger, U.: Hygroscopicity of the submicrometer aerosol at the high-alpine site Jungfraujoch, 3580 m a.s.l., Switzerland, Atmos. Chem. Phys., 8, 5715–5729, doi:10.5194/acp-8-5715-2008, 2008. 8948, 8972
Stohl, A. and Seibert, P.: Accuracy of trajectories as determined from the conservation of meteorological tracers, Q. J. Roy. Meteor. Soc., 124, 1465–1484, 1998. 8950
Stohl, A., Wotawa, G., Seibert, P., and Kromp-Kolb, H.: Interpolation errors in wind fields as a function of spatial and temporal resolution and their impact on different types of kinematic trajectories, J. Appl. Meteorol., 34, 2149–2165, 1995. 8950
Swietlicki, E., Hansson, H., Hämeri, K., Svenningsson, B., Massling, A., McFiggans, G., McMurry, P., Petäjä, T., Tunved, P., Gysel, M., Topping, D., Weingartner, E., Baltensperger, U., Rissler, J., Wiedensohler, A., and Kulmala, M.: Hygroscopic properties of submicrometer atmospheric aerosol particles measured with H-TDMA instruments in various environments – a review, Tellus B, 60, 432–469, 2008. 8960, 8961





ACPD
13, 8939–8984, 2013



Topping, D. O., McFiggans, G. B., and Coe, H.: A curved multi-component aerosol hygroscopicity model framework: Part 1 – Inorganic compounds, Atmos. Chem. Phys., 5, 1205–1222, doi:10.5194/acp-5-1205-2005, 2005. 8948, 8960, 8972

Trenberth, K., Fasullo, J., and Kiehl, J.: Earth's global energy budget, B. Am. Meteorol. Soc., 90, 311–323, 2009. 8940

Twomey, S.: Atmospheric Aerosols, Developments in Atmospheric Science, Elsevier, New York, USA, 1977. 8941

Voss, K., Welton, E., Quinn, P., Frouin, R., Miller, M., and Reynolds, R.: Aerosol optical depth measurements during the Aerosols99 experiment, J. Geophys. Res., 106, 20821–20831, doi:10.1029/2000JD900783, 2001. 8941

Wang, W., Rood, M., Carrico, C., Covert, D., Quinn, P., and Bates, T.: Aerosol optical properties along the northeast coast of North America during the New England Air Quality Study – Intercontinental Transport and Chemical Transformation 2004 campaign and the influence of aerosol composition, J. Geophys. Res., 112, D10S23, doi:10.1029/2006JD007579, 2007. 8942

Weingartner, E., Baltensperger, U., and Burtscher, H.: Growth and structural change of combustion aerosols at high relative humidity, Environ. Sci. Technol., 29, 2982–2986, 1995. 8942

WMO/GAW: Aerosol Measurement Procedures Guidelines and Recommendations, Report No. 153, World Meteorological Organization, Geneva, Switzerland, 2003. 8941

Yan, P., Pan, X., Tang, J., Zhou, X., Zhang, R., and Zeng, L.: Hygroscopic growth of aerosol scattering coefficient: a comparative analysis between urban and suburban sites at winter in Beijing, Particuology, 7, 52–60, 2009. 8942

Zieger, P., Fierz-Schmidhauser, R., Gysel, M., Ström, J., Henne, S., Yttri, K. E., Baltensperger, U., and Weingartner, E.: Effects of relative humidity on aerosol light scattering in the Arctic, Atmos. Chem. Phys., 10, 3875–3890, doi:10.5194/acp-10-3875-2010, 2010. 8942, 8943, 8953, 8954, 8970

Zieger, P., Weingartner, E., Henzing, J., Moerman, M., de Leeuw, G., Mikkilä, J. Ehn, M., Petäjä, T., Clémer, K., van Roozendael, M., Yilmaz, S., Frieß, U. Irie, H., Wagner, T., Shaiganfar, R., Beirle, S., Apituley, A., Wilson, K., and Baltensperger, U.: Comparison of ambient aerosol extinction coefficients obtained from in-situ, MAX-DOAS and LIDAR measurements at Cabauw, Atmos. Chem. Phys., 11, 2603–2624, doi:10.5194/acp-11-2603-2011, 2011. 8941, 8942, 8944, 8946, 8953, 8962, 8970





ACPD
13, 8939–8984, 2013



Zieger, P., Kienast-Sjögren, E., Starace, M., von Bismarck, J., Bukowiecki, N., Baltensperger, U., Wienhold, F. G., Peter, T., Ruhtz, T., Collaud Coen, M., Vuilleumier, L., Maier, O., Emili, E., Popp, C., and Weingartner, E.: Spatial variation of aerosol optical properties around the high-alpine site Jungfraujoch (3580 m a.s.l.), Atmos. Chem. Phys., 12, 7231–7249, doi:10.5194/acp-12-7231-2012, 2012. 8941, 8942, 8946

Zieger, P., Fierz-Schmidhauser, R., Poulain, L., Müller, T., Birmili, W., Spindler, G., Wiedensohler, A., Baltensperger, U., and Weingartner, E.: Influence of water uptake on the aerosol particle light scattering coefficients of the Central European aerosol, J. Geophys. Res., in review, 2013. 8942, 8944, 8970





ACPD
13, 8939–8984, 2013



**Table 1.** Overview of the used instrumentation for the investigated sites.

| Parameter | Employed instrument | Jungfraujoch[a] JFJ | Ny-Ålesund[b] NYA | Mace Head[c] MHD | Melpitz[d] MEL | Cabauw[e] CAB |
|---|---|---|---|---|---|---|
| Particle light scattering coefficient | Humidified nephelometer (WetNeph) | x | x | x | x | x |
| | Nephelometer (DryNeph) | x | x | x | x | x |
| Particle light absorption coefficient | Aethalometer | x | x | x | – | x[f] |
| | Multi-angle absorption photometer (MAAP) | x | – | – | x | x |
| Particle number size distribution | Scanning mobility particle sizer (SMPS) | x | x | x | – | x[f] |
| | Dual mobility particle size spectrometer (DMPSS) | – | – | – | x | – |
| | Optical particle size spectrometer (OPSS) | x | x | x | x | – |
| | Aerodynamic particle sizer (APS) | – | – | – | – | x |
| Hygroscopic growth factor | Hygroscopic tandem differential mobility analyzer (H-TDMA) | x[f] | – | x | x[f] | x[f] |
| Chemical composition | Aerosol mass spectrometer (AMS) | x | – | – | x | – |
| | Filter measurements | – | x | – | x | – |
| Location | | Switzerland 46.55° N, 7.98° E 3580 m a.s.l. | Spitsbergen 78.92° N, 11.94° E 475 m a.s.l. | Ireland 53.33° N, 9.91° W 5 m a.s.l. | Germany 51.53° N, 12.92° E 86 m a.s.l. | the Netherlands 51.97° N, 4.93° E 1 m a.s.l. |
| Time period (days) | | May 2008 (31) | Jul–Oct 2008 (91) | Jan–Feb 2009 (28) | Feb–Mar 2009 (36) | Jun–Oct 2009 (120) |

[a] Fierz-Schmidhauser et al. (2010b).
[b] Zieger et al. (2010).
[c] Fierz-Schmidhauser et al. (2010c).
[d] Zieger et al. (2013).
[e] Zieger et al. (2011).
[f] Data only partly available.





ACPD
13, 8939–8984, 2013



**Table 2.** Mean, standard deviation (STD) and percentile values of $f(\mathrm{RH} = 85\,\%, 550\,\mathrm{nm})$ for the Jungfraujoch (JFJ), Ny-Ålesund (NYA), Mace Head (MHD), Melpitz (MEL), and Cabauw (CAB). Average values are also given for different air mass types, if a differentiation of specific air masses was possible during the individual measurement periods.

| Station: Type | Mean | STD | 75th prctl. | Median | 25th prctl. |
|---|---|---|---|---|---|
| JFJ: All | 2.30 | 0.33 | 2.52 | 2.34 | 2.12 |
| JFJ: Free tropospheric/PBL influenced | 2.32 | 0.31 | 2.53 | 2.35 | 2.13 |
| JFJ: Saharan dust influenced | 1.28 | 0.10 | 1.35 | 1.27 | 1.20 |
| NYA: All | 3.24 | 0.63 | 3.63 | 3.12 | 2.79 |
| NYA: Sea salt | 2.86 | 0.41 | 3.05 | 2.81 | 2.56 |
| NYA: Arctic (no sea salt) | 3.41 | 0.66 | 3.71 | 3.28 | 3.05 |
| MHD: All | 2.08 | 0.29 | 2.30 | 2.11 | 1.87 |
| MHD: Clean sector (sea salt) | 2.28 | 0.19 | 2.37 | 2.29 | 2.17 |
| MHD: Polluted sector | 1.80 | 0.26 | 1.96 | 1.82 | 1.66 |
| MEL: All | 2.77 | 0.37 | 3.02 | 2.78 | 2.56 |
| CAB: All | 2.38 | 0.38 | 2.63 | 2.34 | 2.14 |
| CAB: Maritime | 3.38 | 0.31 | 3.60 | 3.38 | 3.16 |
| CAB: Continental south | 1.86 | 0.17 | 2.02 | 1.86 | 1.76 |
| CAB: Maritime heavily polluted | 1.95 | 0.14 | 2.04 | 2.00 | 1.82 |
| CAB: Maritime slightly polluted | 2.97 | 0.20 | 3.11 | 2.96 | 2.81 |
| CAB: Continental east | 2.25 | 0.16 | 2.37 | 2.26 | 2.13 |





ACPD
13, 8939–8984, 2013



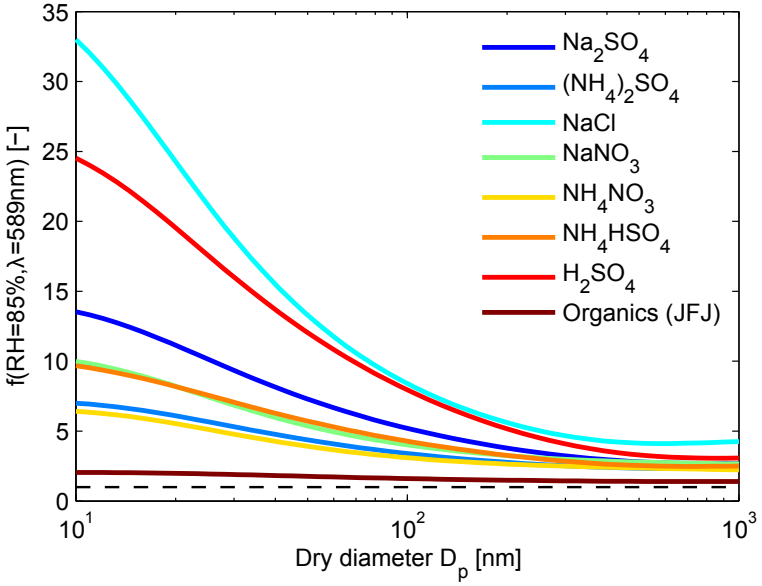


**Fig. 1.** The scattering enhancement $f(\mathrm{RH})$ at $\mathrm{RH} = 85\,\%$ and $\lambda = 589\,\mathrm{nm}$ vs. dry particle diameter calculated for different inorganic salts (see legend) and for organics (typically found at the Jungfraujoch, JFJ). A monomodal size distribution is assumed ($\sigma = 1.8$). The hygroscopic growths factors were taken from Topping et al. (2005); Sjogren et al. (2008) and the refractive indices from Seinfeld and Pandis (2006) and Nessler et al. (2005a).





ACPD
13, 8939–8984, 2013



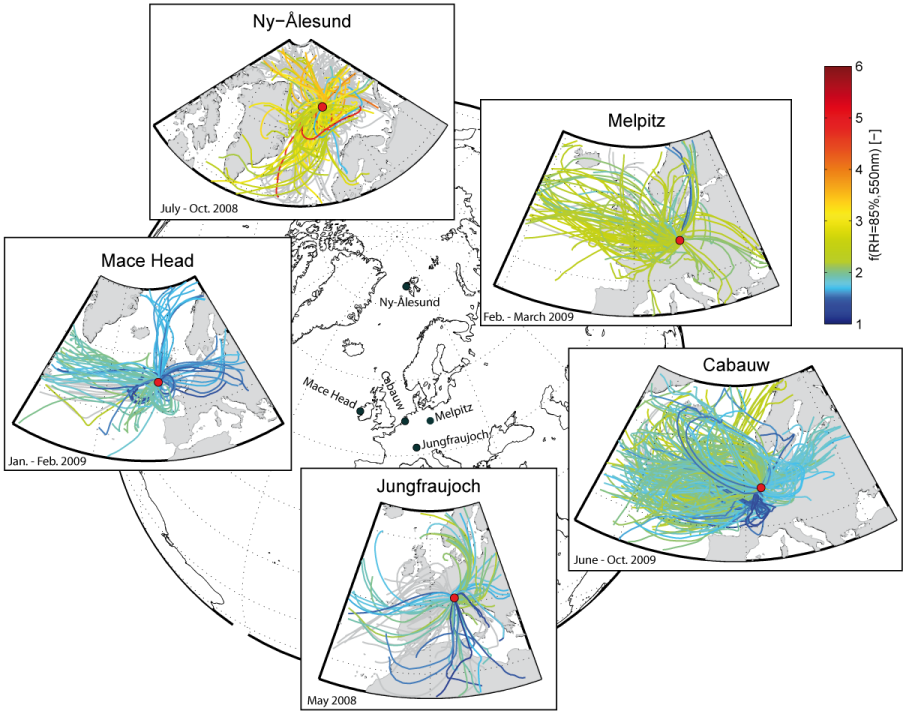


**Fig. 2.** 72 h air mass back trajectories (FLEXTRA) color coded by the $f(\mathrm{RH} = 85\,\%, 550\,\mathrm{nm})$ measured at the time the air parcel arrived at the site.





ACPD
13, 8939–8984, 2013



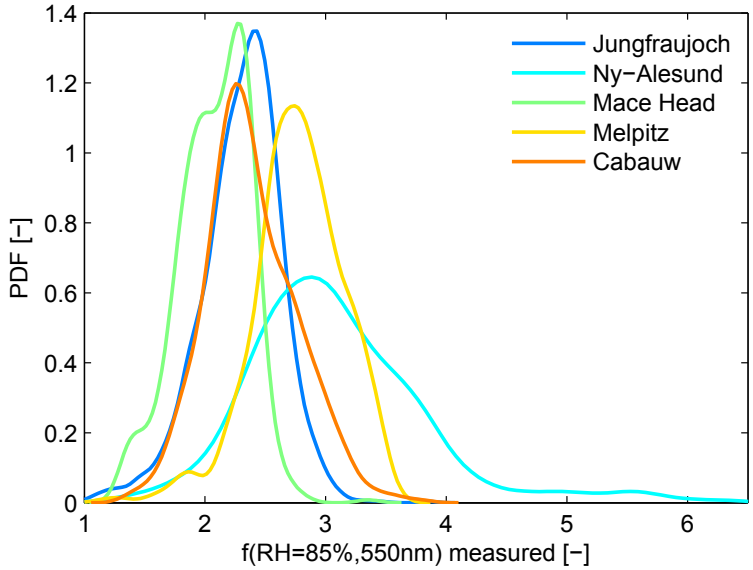


**Fig. 3.** Probability density function (PDF) of measured scattering enhancement $f$(RH = 85 %, 550 nm) at the different sites (see legend).





ACPD
13, 8939–8984, 2013



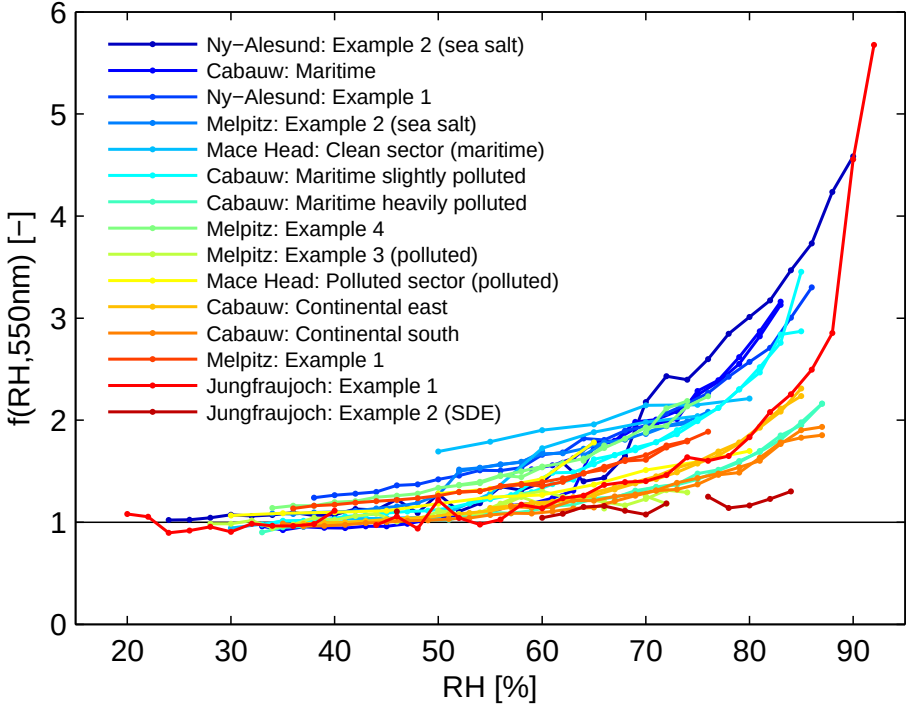


**Fig. 4.** Example humidograms of $f(\mathrm{RH})$ at $\lambda = 550\,\mathrm{nm}$ from the different sites with respect to different air masses (see legend).





ACPD
13, 8939–8984, 2013



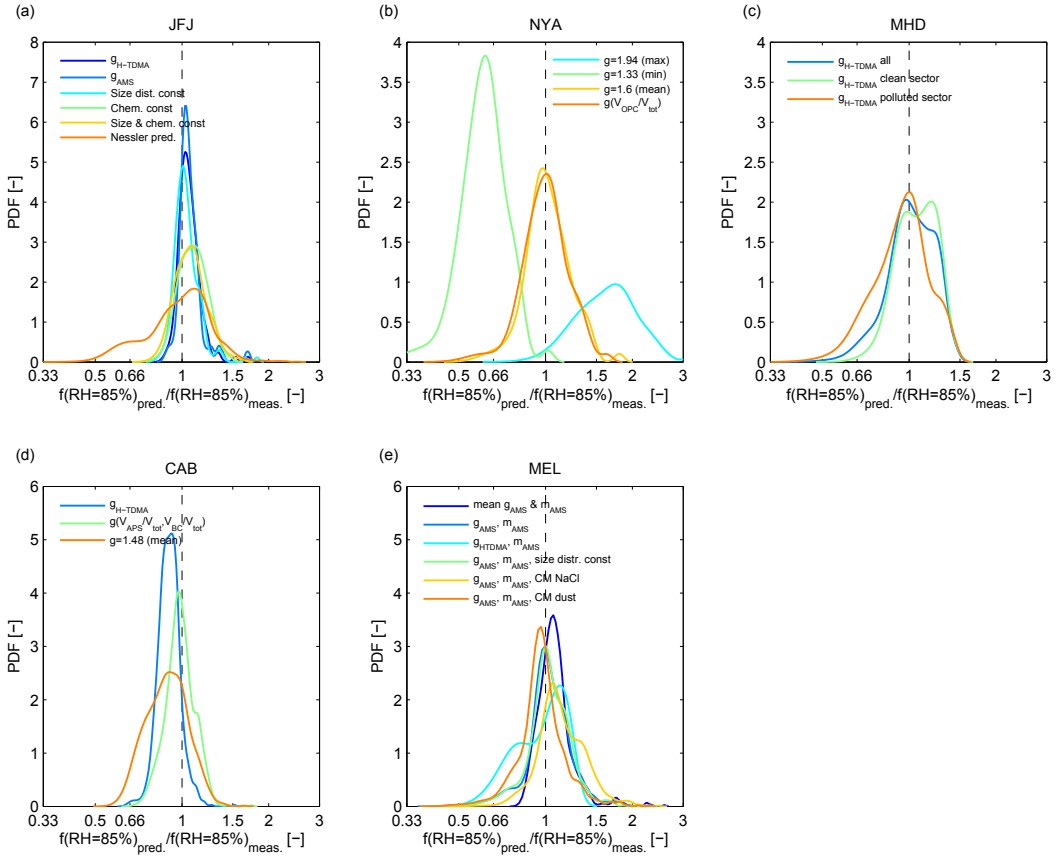


**Fig. 5.** Probability density function (PDF) of predicted to measured $f$(RH = 85 %, 550 nm) of the individual closure studies, which were characterized with their own specific settings (see text).





ACPD
13, 8939–8984, 2013



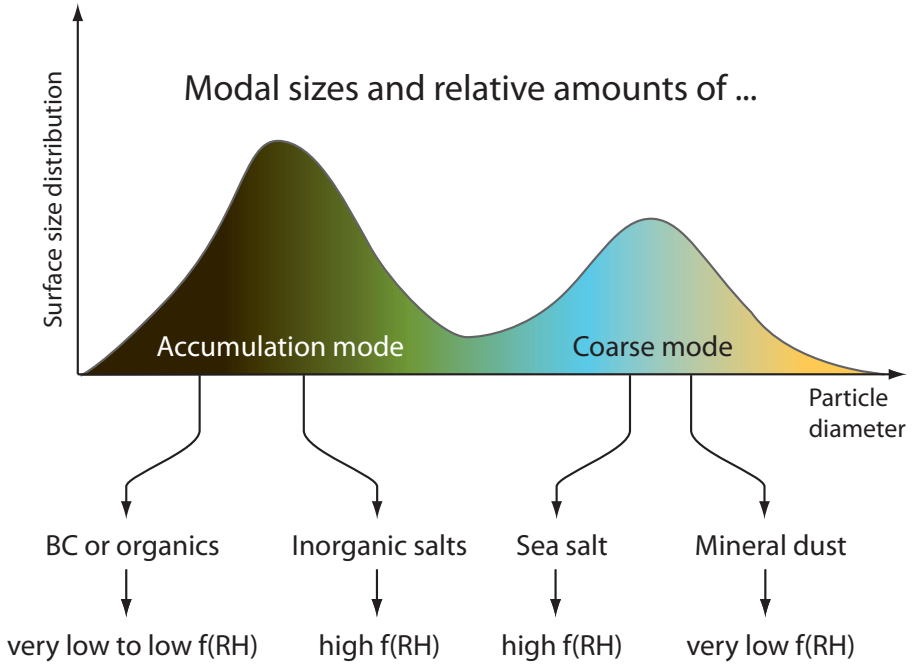


**Fig. 6.** Schematic overview on the factors influencing the scattering enhancement $f$(RH). The size and the relative contributions of the different modes with its distinct chemical composition (governing the hygroscopic growth and refractive index) are all influencing $f$(RH). This does also include compensating effects of size and chemical composition.





ACPD
13, 8939–8984, 2013



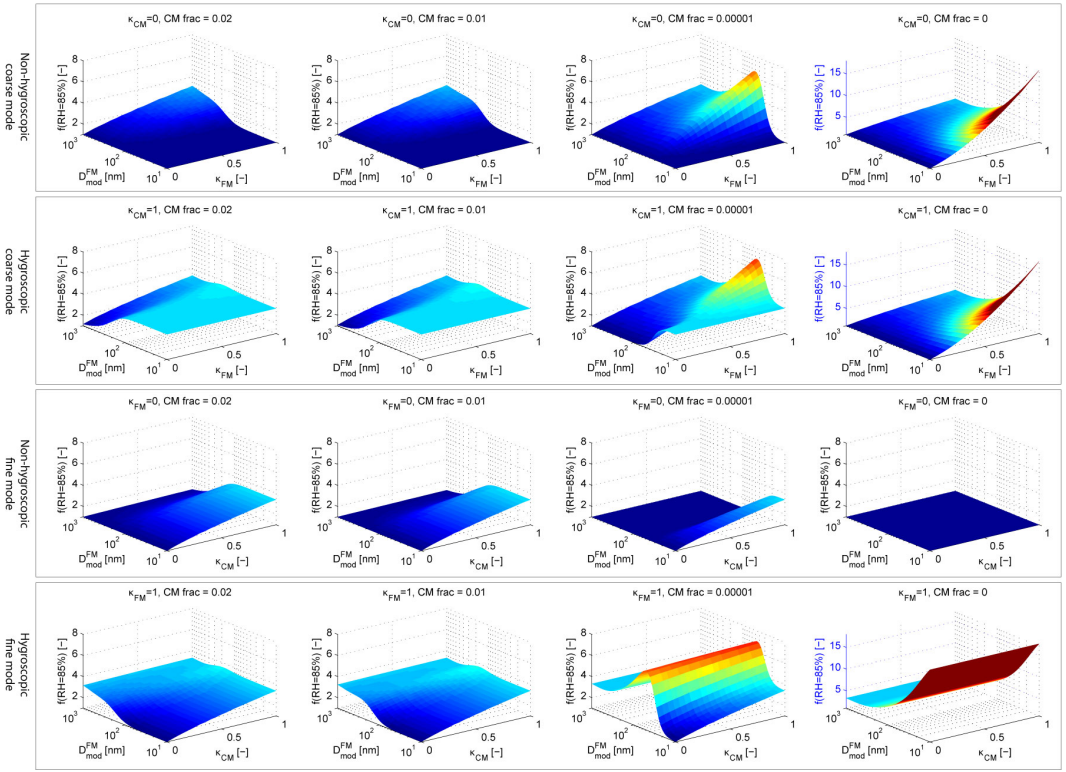


**Fig. 7.** The scattering enhancement $f(\mathrm{RH})$ at RH = 85 % and $\lambda$ = 550 nm modeled for different coarse mode (CM) fractions, fine mode (FM) mode diameters and hygroscopicities. A refractive index of $m$ = 1.54 and a mode width of $\sigma$ = 1.8 for fine and coarse mode of the lognormal size distribution is assumed. The mode diameter of the coarse mode is assumed to be constant at $D$ = 2 µm. Note the different scale of the z-axis for the monomodal case (CM = 0, blue axis).





ACPD
13, 8939–8984, 2013



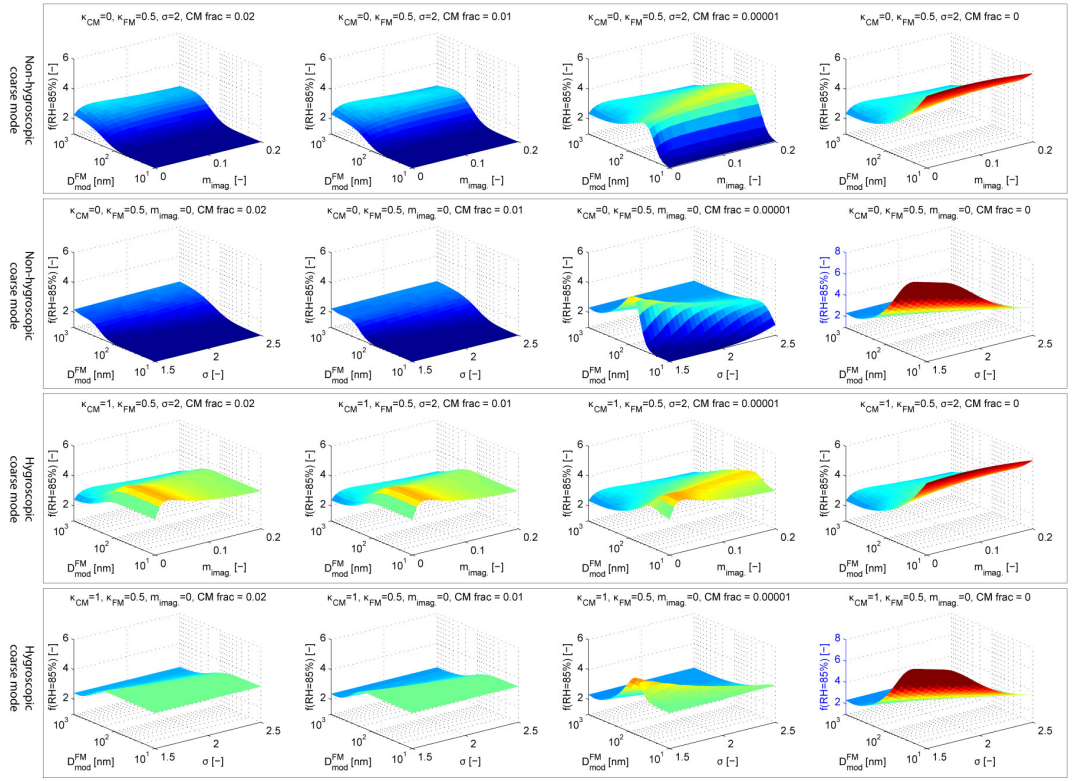


**Fig. 8.** Same as Fig. 7 but for varying imaginary parts of the refractive index and varying width of the fine mode.





ACPD
13, 8939–8984, 2013

Effects of relative humidity on aerosol light scattering

P. Zieger et al.



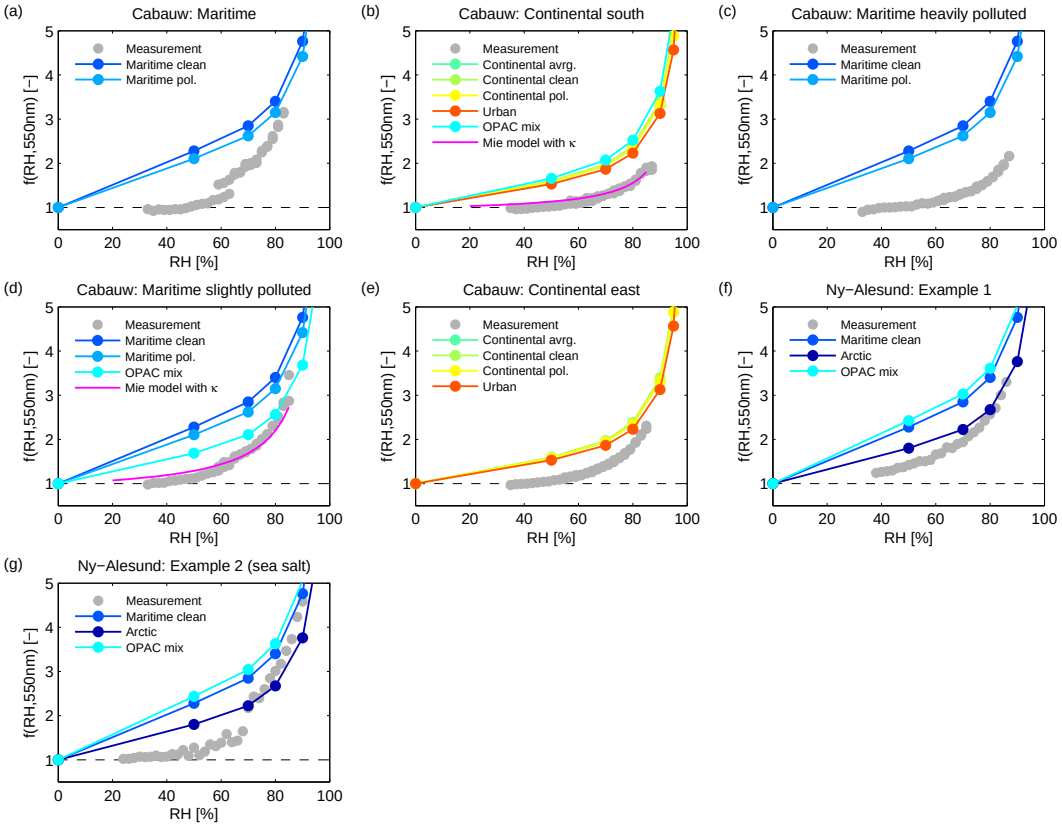


**Fig. 9.** Example humidograms from the investigated sites (gray bullets) compared to OPAC aerosol examples given in Hess et al. (1998) (colored bullet lines). The cyan bullets (OPAC mix) denote the OPAC result if the individual OPAC components are weighted with the measured size distribution. The magenta line shows the calculated humidogram using the measured size distribution, the (partially) measured chemical composition, the hygroscopicity parameter $\kappa$ and applying Mie calculations if the measurements were available (see text for details).





ACPD
13, 8939–8984, 2013



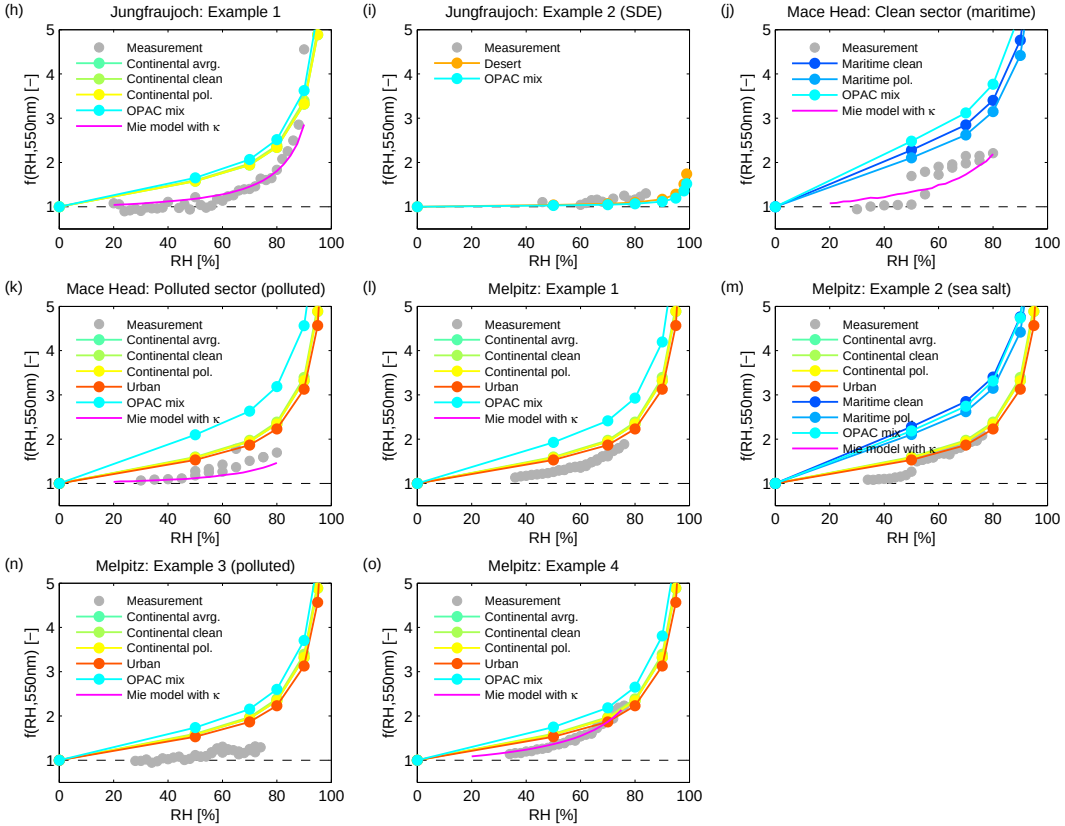


**Fig. 10.** Same as Fig. 9 for the other sites.





ACPD
13, 8939–8984, 2013



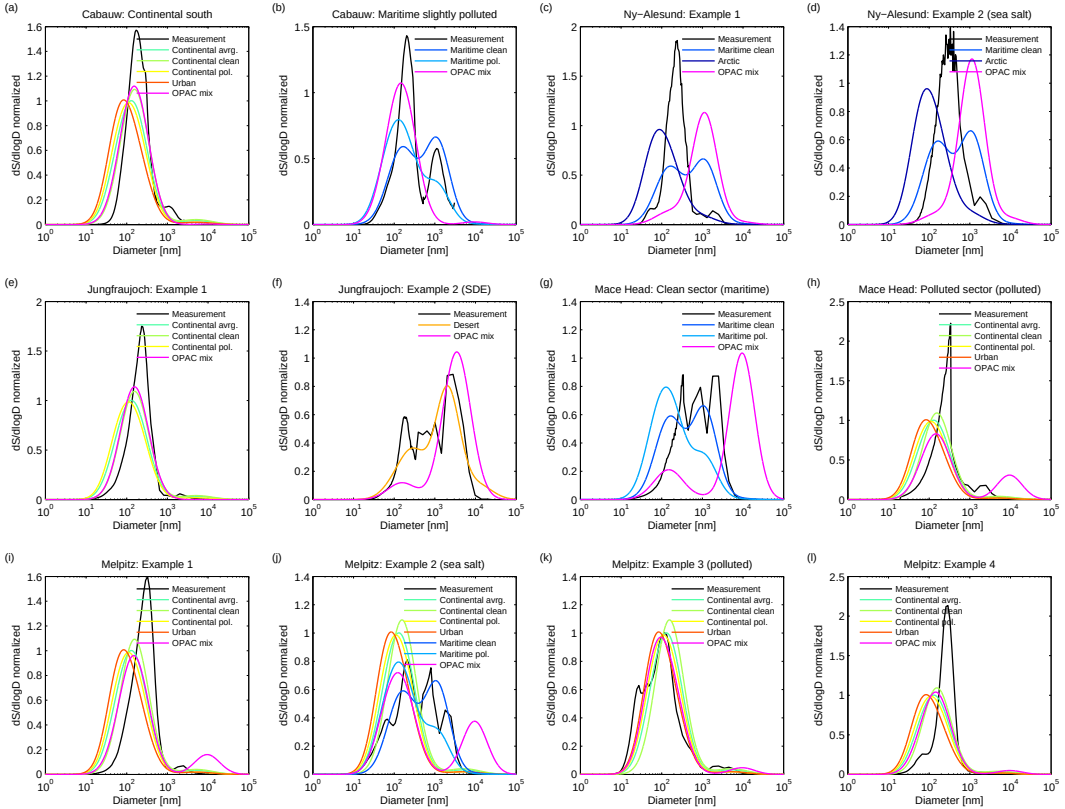


**Fig. 11. (a–f)**: normalized surface size distributions measured (black line) during the humidogram times as shown in Fig. 9 and 10, normalized surface size distributions from the OPAC aerosol type examples (colored lines), and the OPAC size distributions if the individual components are weighted with the measured number size distribution (magenta line). Note that the OPAC components have a fixed mode diameter and therefore the OPAC individually mixed size distributions do not match the measured distribution in all cases.





ACPD
13, 8939–8984, 2013

Effects of relative humidity on aerosol light scattering

P. Zieger et al.



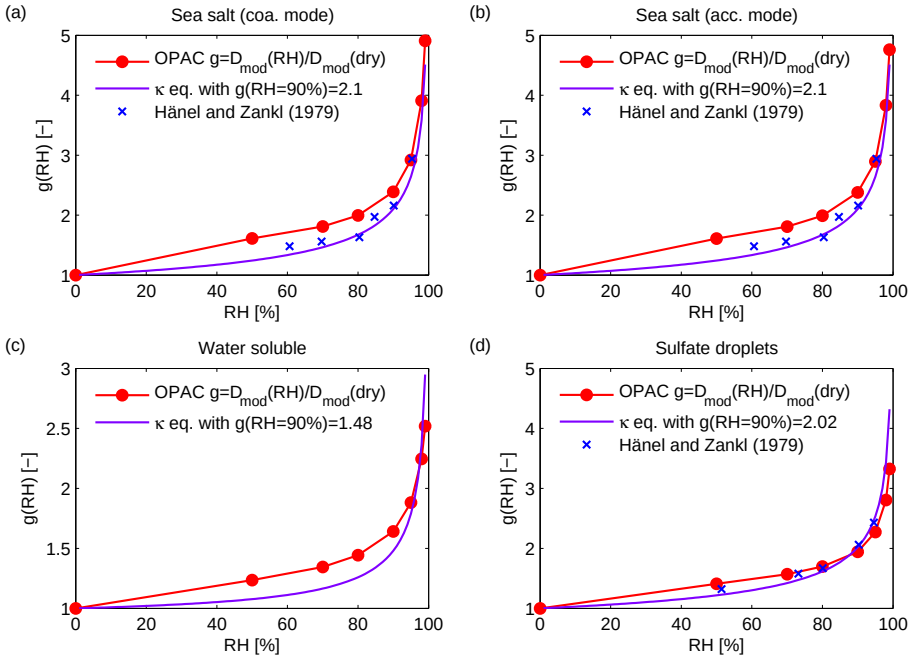


**Fig. 12.** Hygroscopic growth factor $g$(RH) as implemented for the four hygroscopic OPAC components. **(a)** Sea salt (accumulation mode), **(b)** sea salt (coarse mode), **(c)** water-soluble, **(d)** sulfate droplets (used to model Antarctic and stratospheric background aerosol). The mode diameter (red curve) growth factors used for the individual lognormal size distributions are shown. The violet curve denotes the hygroscopic growth factor as calculated using literature values of $g$(RH) and the $\kappa$-equation (see text for details). The blue crosses show the original $g$(RH) from Hänel and Zankl (1979).





ACPD
13, 8939–8984, 2013



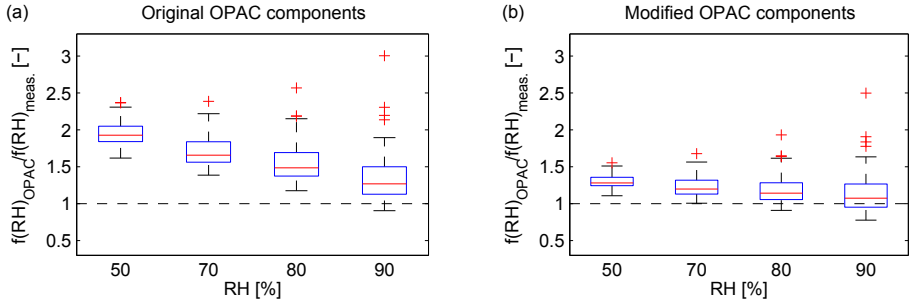


**Fig. 13.** Box plots of the ratio of calculated to measured $f$(RH) (at 550 nm) for the RH values of 50, 70, 80, and 90 % (OPAC values and range of measurements) for Cabauw (4–18 July 2009). The central red mark is the median, the edges of the box are the 25th and 75th percentiles, the error bars show the extent to the most extreme data points that are not considered as outliers, while the outliers are plotted individually (red crosses). **(a)** $f$(RH) calculated using the original OPAC components weighted with the measured size distribution. **(b)** $f$(RH) calculated using the modified OPAC components (changed hygroscopic growth) weighted with the measured size distribution.





ACPD
13, 8939–8984, 2013